

EFFECTS OF PULSAR ROTATION ON TIMING MEASUREMENTS OF THE DOUBLE PULSAR SYSTEM J0737-3039

ROMAN R. RAFIKOV¹ AND DONG LAI²

Draft version November 6, 2018

ABSTRACT

We study the effect of pulsar rotation on timing of binary pulsars, with particular emphasis on the double pulsar system J0737-3039. Special relativistic aberration due to the orbital motion of pulsar changes both the longitude and latitude of the emission direction with respect to the pulsar spin axis. The former gives rise to a shift of the arrival time of the pulse centroid (this is the conventional “longitudinal” aberration delay), the latter results in a distortion (contraction or dilation) of the pulse profile on the orbital timescale. In the framework of the rotating vector model of pulsar emission, the amplitude of pulse distortion depends inversely on the variation of polarization position angle across the pulse. For small angle between the pulsar magnetic and spin axes, as inferred for PSR J0737-3039A from polarimetric observations, the pulse distortion is significant ($\sim 1\%$) and the associated “latitudinal” aberration delay is much larger than the longitudinal one. We show that by monitoring the arrival time of separate pulse components as a function of pulsar orbital phase, the latitudinal aberration delay may be easily measured with the current timing precision. Such measurement would constrain the spin geometry of the system. The latitudinal delay can also be detected by monitoring system’s orbital parameters on the geodetic precession timescale. Because of the near edge-on orbital orientation of the PSR J0737-3039 system, general relativistic bending of pulsar A’s radio beam near its superior conjunction also introduces spin-dependent time delays of similar order of magnitude as the aberration delays. In addition, light bending splits the pulse profile into two variable components, corresponding to two gravitationally lensed images of the source. Detection of lensing effects is challenging, but may be possible with existing technology.

Subject headings: pulsars: general — stars: neutron — pulsars: individual (J0737-3039A, J0737-3039B) — gravitational lensing — binaries: general

1. INTRODUCTION

The recently discovered double pulsar system J0737-3039 (Burgay et al. 2003; Lyne et al. 2004) presents an unprecedented natural laboratory for testing our understanding of general relativity and pulsar magnetosphere physics. One of the unique features of this system is the almost edge-on orientation of its orbital plane with respect to our line of sight. Currently the two best constraints on the system’s inclination come from the Shapiro delay ($i = 88.7^\circ \pm 0.9^\circ$; Lyne et al. 2004; Ransom et al. 2004) and from scintillation measurements ($|i - 90^\circ| = 0.29^\circ \pm 0.14^\circ$, Coles et al. 2004). Among other effects this high inclination leads to periodic eclipses of the millisecond pulsar (pulsar A) by plasma in the magnetosphere of the normal pulsar (pulsar B) (see Lyne et al. 2004; Kaspi et al. 2004; McLaughlin et al. 2004; Arons et al. 2004; Rafikov & Goldreich 2004; Lyutikov & Thompson 2005).

The edge-on orientation of the system also makes possible gravitational light bending of the pulsar signal when the pulsar passes through its superior conjunction with respect to the companion. In Lai & Rafikov (2005), we studied the effect of gravitational lensing on the pulse intensity and the impact of light bending on the correlated scintillation measurements of both pulsars. We also evaluated the effects of light bending on the pulse arrival time: geometric time delay and the modified Shapiro de-

lay — both of these timing contributions are independent of the pulsar spin.

Since pulsar signals are due to the beamed emission of a rotating neutron star (as opposed to radial pulsation of the star), additional spin-dependent time delays arise due to special relativistic aberration (Smarr & Blandford 1976; Damour & Deruelle 1986) and general relativistic light bending (cf. Schneider 1990). The goal of this paper is to evaluate these spin-dependent delays in the PSR J0737-3039 system, and assess their detectability and potential for constraining the parameters of the system. We also examine the distortion of pulse profile due to aberration and lensing, and discuss an alternative way of analyzing pulse arrival time and introduce the concept of “latitudinal delay” that focuses on specific features in the pulse profile. For PSR J0737-3039, a measurement of this latitudinal delay may lead to useful constraints on the geometry of the system.

In §2, we calculate the spin-dependent time delays due to aberration and lensing. In §3, we examine the pulse shape distortion/variation and calculate the latitudinal delays. The prospects of detecting these effects are discussed in §4.

Although the formulae derived in this paper are general for any binary pulsar system, we shall apply them to PSR J0737-3039, concentrating on the effects of rotational delays on the timing of the millisecond pulsar A, with pulsar B playing the role of the lensing companion. We adopt the following parameters for the system: $M_p = M_A = 1.337M_\odot$, $M_c = M_B = 1.25M_\odot$, the spin period of pulsar A $P_A = 22.7$ ms, the or-

¹ IAS, Einstein Dr., Princeton, NJ 08540; rrr@ias.edu

² Department of Astronomy, Cornell University, Ithaca, NY 14853; dong@astro.cornell.edu

bit period $P_b = 0.1023$ d, the orbital semimajor axis $a = 8.784 \times 10^{10}$ cm, eccentricity $e = 0.0878$, longitude of periastron $\omega = 73.8^\circ$ (as of 2004), and the orbital inclination angle i in the range between 90.14° and 90.56° .

2. SPIN-DEPENDENT TIME DELAYS

Because of special relativistic light aberration, the direction of emission in the comoving frame of the pulsar, \mathbf{N} ($|\mathbf{N}| = 1$), differs from that in the observer's frame, \mathbf{n} ($|\mathbf{n}| = 1$), by the vector

$$(\Delta\mathbf{n})_A = \mathbf{n} \times (\mathbf{n} \times \boldsymbol{\beta}_p) \simeq \mathbf{n}_0 \times (\mathbf{n}_0 \times \boldsymbol{\beta}_p), \quad (1)$$

where $\mathbf{v}_p = c\boldsymbol{\beta}_p$ is the pulsar velocity relative to the binary barycenter³, and \mathbf{n}_0 is the unit vector from the binary system to the observer. Because of general relativistic light bending, the direction of emission \mathbf{n} at the pulsar position differs from \mathbf{n}_0 . This lensing effect is important only around the superior conjunction of the pulsar, giving rise to potentially measurable time delay provided that the minimum projected separation between the pulsar and its companion is comparable to the companion's Einstein radius (Lai & Rafikov 2005). The deflection vector due to light bending $(\Delta\mathbf{n})_L = \mathbf{n} - \mathbf{n}_0$ is given by⁴

$$(\Delta\mathbf{n})_L = \left(\frac{\Delta R_\pm}{R}\right) \frac{\mathbf{R}}{a_\parallel} = \left(\frac{\Delta R_\pm}{R}\right) \frac{\mathbf{n}_0 \times (\mathbf{r} \times \mathbf{n}_0)}{a_\parallel}. \quad (2)$$

Here $\mathbf{r} = \mathbf{r}_p - \mathbf{r}_c$ is the position vector of the pulsar relative to its companion, $\mathbf{R} = \mathbf{n}_0 \times (\mathbf{r} \times \mathbf{n}_0)$ is the projection of \mathbf{r} in the sky plane, $R = |\mathbf{R}| = r(1 - \sin^2 i \sin^2 \psi)^{1/2}$ (ψ is the true anomaly measured from the ascending node of the pulsar), $r = a(1 - e^2)/(1 + e \cos \phi)$ is the distance between pulsar and its companion ($\phi = \psi - \omega$ is the orbital true anomaly measured from periastron), and $a_\parallel = a \sin i(1 - e^2)/(1 + e \sin \omega)$ is this distance at the conjunction projected along our line of sight (a, e and ω are the orbital semimajor axis, eccentricity, and longitude of periastron, respectively). Gravitational lensing gives rise to two pulsar images (specified by the subscript “ \pm ”); ΔR_\pm is the displacement (in the sky plane) of the image position, $\mathbf{R}_\pm = (\Delta R_\pm/R + 1)\mathbf{R}$, relative to the fiducial position, \mathbf{R} , and is given by

$$\Delta R_\pm = \frac{1}{2} \left(\pm \sqrt{R^2 + 4R_E^2} - R \right), \quad (3)$$

with the Einstein radius

$$R_E = (2R_g a_\parallel)^{1/2} \simeq (2R_g a)^{1/2} = 2550 \text{ km}. \quad (4)$$

Here $R_g = 2GM_c/c^2 = 3.69$ km and the numerical value is for J0737-3039A with pulsar B playing role of the companion. Combining eqs. (1) and (2), the direction of emission in the pulsar's comoving frame is $\mathbf{N} = \mathbf{n}_0 + \Delta\mathbf{N}$, with $\Delta\mathbf{N} = (\Delta\mathbf{n})_A + (\Delta\mathbf{n})_L$. The deflection angle of the

³ The constant velocity of the barycenter itself does not affect timing measurement.

⁴ Analogous to the classical work of Damour & Taylor (1992), our calculations of the lensing effects are performed in the static limit, which neglects the change in the position of the companion during the time it takes the photon to cross the binary. Including this propagation effect in the spirit of Kopeikin & Schäfer (1999) would not qualitatively change our conclusions and we omit it from the present consideration for the purposes of clarity.

emission vector due to light bending, $\Delta R/a$, has a maximum value (for the “plus” image) $R_E/a \sim v/c$ (this occurs at the orbital conjunction and $i = 90^\circ$), which is of the same order as the aberration effect. This similarity of the magnitudes of two effects holds only in the binary systems which are so highly inclined with respect to our line of sight that $R \sim R_E$ at conjunction (in more face-on systems with $\cos i \sim 1$ the gravitational light deflection is a $(v/c)^2$ effect).

Variation of the emission direction \mathbf{N} causes a shift in the equatorial longitude Φ of \mathbf{N} in the corotating frame of pulsar (counted in the direction of rotation) given by

$$\Delta\Phi = \frac{\Delta\mathbf{N} \cdot (\mathbf{s}_p \times \mathbf{n}_0)}{|\mathbf{s}_p \times \mathbf{n}_0|^2}, \quad (5)$$

where \mathbf{s}_p is the unit vector along the pulsar spin axis. For an arbitrary emission pattern rigidly rotating around \mathbf{s}_p , any change in the equatorial longitude corresponds to a change of emission phase, leading to a time delay $\Delta t = \Delta\Phi/\Omega_p = (\Delta t)_A + (\Delta t)_L$ (here Ω_p is the angular frequency of the pulsar and the time delay is positive for signal arriving later), where

$$(\Delta t)_A = -\frac{\boldsymbol{\beta}_p \cdot (\mathbf{s}_p \times \mathbf{n}_0)}{\Omega_p |\mathbf{s}_p \times \mathbf{n}_0|^2}, \quad (6)$$

$$(\Delta t)_L = \left(\frac{\Delta R_\pm}{R}\right) \frac{\mathbf{r} \cdot (\mathbf{s}_p \times \mathbf{n}_0)}{\Omega_p a_\parallel |\mathbf{s}_p \times \mathbf{n}_0|^2} \quad (7)$$

are contributions due to aberration (Smarr & Blandford 1975) and gravitational light bending (cf. Schneider 1990)⁵, respectively. Note that this “longitudinal” time delay shifts the whole pulse profile uniformly without introducing any distortions to its shape (see §3).

The pulsar spin axis \mathbf{s}_p is specified by two angles (see Fig. 1 of Damour & Taylor 1992; thereafter DT92): ζ is the angle between \mathbf{s}_p and the light-of-sight vector \mathbf{n}_0 , and η is the angle between the ascending node of the orbit and the projection of \mathbf{s}_p on the sky plane. The aberration time delay (6) is then given by

$$(\Delta t)_A = A(\sin \psi + e \sin \omega) + B(\cos \psi + e \cos \omega), \quad (8)$$

with

$$\begin{Bmatrix} A \\ B \end{Bmatrix} = -\frac{\Omega_b a_p}{\Omega_p c \sqrt{1 - e^2} \sin \zeta} \begin{Bmatrix} \sin \eta \\ \cos i \cos \eta \end{Bmatrix}, \quad (9)$$

where $\Omega_b = (GM_t/a^3)^{1/2}$ ($M_t = M_p + M_c$ is the total mass of the system) and $a_p = (M_c/M_t)a$. These expressions coincide with the results of Damour & Deruelle (1986) and DT92 (expressed in terms of a complementary angle $\lambda = \pi - \zeta$ instead of ζ). Similarly, the delay associated with light bending is

$$\begin{aligned} (\Delta t)_L &= -\left(\frac{\Delta R_\pm}{R}\right) \left(\frac{r}{a_\parallel}\right) \frac{\sin \eta \cos \psi - \cos i \cos \eta \sin \psi}{\Omega_p \sin \zeta} \\ &= -\left(\frac{\Delta R_\pm}{a_\parallel \Omega_p}\right) \frac{(\sin \eta \cos \psi - \cos i \cos \eta \sin \psi)}{\sin \zeta (1 - \sin^2 i \sin^2 \psi)^{1/2}}. \end{aligned} \quad (10)$$

Note that the lensing effect is important only around the orbital conjunction ($\psi = \pi/2$) for nearly edge-on

⁵ This agrees with with expression of Schneider (1990) if we replace a_\parallel by $\mathbf{r} \cdot \mathbf{n}_0 = r \sin i \sin \psi$ — this would lead to divergence at $\psi = 0, \pi$, which is naturally avoided in our case.

systems. Let $i = \pi/2 + \Delta i$ and $\psi = \pi/2 + \Delta\psi$, with $|\Delta i|, |\Delta\psi| \ll 1$, then we have

$$(\Delta t)_L \simeq - \left(\frac{\Delta R_{\pm}}{a_{\parallel} \Omega_p} \right) \frac{\Delta i \cos \eta - \Delta\psi \sin \eta}{\sin \zeta [(\Delta i)^2 + (\Delta\psi)^2]^{1/2}}, \quad (11)$$

with ΔR_{\pm} given by eq. (3) and $R \simeq a_{\parallel} [(\Delta i)^2 + (\Delta\psi)^2]^{1/2}$. Both eqs. (7) and (10) differ from the result of Doroshenko & Kopeikin (1995) (also quoted in Wex & Kopeikin 1999) since these authors used the equation for the light ray trajectory from Klioner & Kopeikin (1992) obtained under the assumption of $R \gg R_E$. As a result, in the most interesting case when $R \sim R_E$ (and bending delay attains its maximum value) the expression for $(\Delta t)_L$ obtained by Doroshenko & Kopeikin (1995) is not applicable and cannot be used for interpreting timing measurements⁶. Also note that some previous treatments of bending delay (e.g. Goicoechea et al. 1995) were restricted to circular and/or purely edge-on orbits.

Neglecting the dependence on various angles, the aberration time delay is of order $\Omega_b a_p / (c \Omega_p) = 3.6 \mu\text{s}$, and the rotational lensing delay at the conjunction is of order $\Delta R_{\pm} / (a_{\parallel} \Omega_p) = 10.5 (\Delta R_{\pm} / R_E) \mu\text{s}$. Not surprisingly, the two delays are of the same order of magnitude at the conjunction, since $\Omega_b a_p \sim v_p / c \sim v / (2c)$ and $R_E / a \sim \sqrt{2} v / c$.

Damour and Deruelle (1986) recognized that the aberration delay is degenerate with the Roemer delay, and therefore cannot be directly measured (but see §4). The time delays associated with lensing do not suffer from this degeneracy. Figures 1 and 2 show these delays (the combined geometric and Shapiro delays as calculated in Lai & Rafikov (2005), and the rotational lensing delay given by eq. [10] or [11]) together with the amplification factor for both images,

$$A_{\pm} = \frac{u^2 + 2}{2u\sqrt{u^2 + 4}} \pm \frac{1}{2}, \quad u = R/R_E. \quad (12)$$

In evaluating $(\Delta t)_L$, we adopt $\zeta = 50^\circ$ as suggested by Demorest et al. (2004) from polarization measurement (although this angle is currently unconstrained) and use $\eta = 45^\circ$ as an example in Figures 1 and 2.

One can see from Figure 1 that near conjunction the lensing delay associated with positive image reaches $\approx 6 \mu\text{s}$ for $i = 90.28^\circ$. In binary systems with smaller inclination angles the timing signal due to lensing is weaker. One can show that if the minimum projected separation of pulsar from its companion $a_{\parallel} |\Delta i| \gg R_E$ then for $e \ll 1$ the maximum amplitude of $(\Delta t)_L$ is

$$\max |(\Delta t)_L| \approx \frac{(R_E / a_{\parallel})^2}{2 |\Delta i| \Omega_p \sin \zeta} (1 + |\cos \eta|), \quad (13)$$

reached at $\Delta\psi \approx \Delta i (\cos \eta \mp 1) / \sin \eta$, where the upper sign corresponds to $\cos \eta > 0$, while the lower one to $\cos \eta < 0$. Note that increasing $|\Delta i|$ diminishes $\max |(\Delta t)_L|$ no faster than $|\Delta i|^{-1}$. The orbital phase at which this maximum occurs shifts from conjunction in proportion to $|\Delta i|$ reducing magnetospheric absorption effects in systems with larger $|\Delta i|$. In particular, if

⁶ By contrast, our expression is valid for all R as long as $R \ll a_{\parallel}$. For $R \sim a_{\parallel}$, the lensing effect is completely negligible.

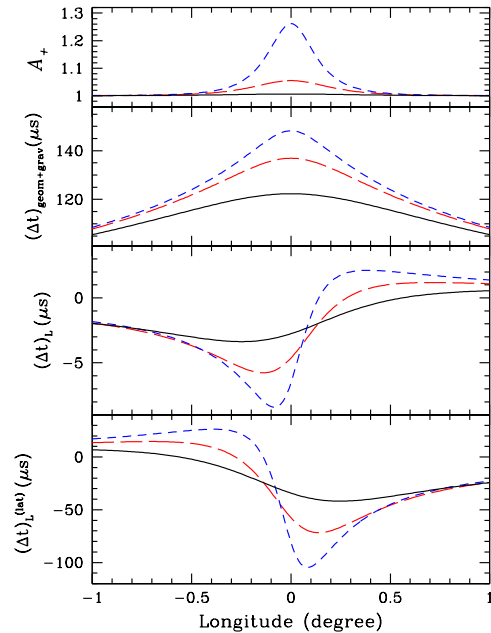


FIG. 1.— The amplification (top panel), the combined geometric and gravitational (Shapiro) delay (the second panel), the rotational lensing delay (the third panel), and the latitudinal lensing delay (the bottom panel) of the dominant (“plus”) image of the pulsar A signal as a function of the orbital phase. The longitude is measured from the superior conjunction of pulsar A (when A is exactly behind pulsar B). In each panel, the inclination angles are $i = 90.56^\circ$ (solid line), 90.28° (long-dashed line) and 90.14° (short-dashed line). For the third and bottom panels, the angles $\zeta = 50^\circ$, $\eta = 45^\circ$ and $\tan \chi_0 = 0.08$ are used.

the real inclination angle of J0737-3039 is closer to that measured with the Shapiro delay ($i = 88.7^\circ$) rather than the one inferred using the scintillation technique, then $\max |(\Delta t)_L|$ amounts to $\approx 1.7 \mu\text{s}$ (which is at present unmeasurable) reached ≈ 13 s after conjunction, which is almost at the end of eclipse of pulsar A.

The magnitude of $(\Delta t)_L$ scales as $(\sin \zeta)^{-1}$ and its shape depends on η as $(\Delta i) \cos \eta - (\Delta\psi) \sin \eta$. As a result, unlike the geometric delay and Shapiro delay, the rotational lensing delay is generally *asymmetric* with respect to orbital conjunction (the exception is when $\eta = 0, 180^\circ$). Note that although the delays associated with the “minus” image can become very large (100’s of μs) as a result of its large deflection ($|\Delta R_- / a_{\parallel}|$), this image is usually too demagnified to be of interest (see §3.3.3).

3. PULSE PROFILE VARIATION AND “LATITUDINAL TIME DELAY”

3.1. Pulse Profile Variation

Variation of the pulse emission direction \mathbf{N} also results in the change of colatitude of emission vector, ζ . Since $\cos \zeta = \mathbf{s}_p \cdot \mathbf{N}$ and $\sin \zeta = |\mathbf{s}_p \times \mathbf{N}|$, we find

$$\Delta \zeta = - \frac{\mathbf{s}_p \cdot \Delta \mathbf{N}}{|\mathbf{s}_p \times \mathbf{n}_0|} = (\Delta \zeta)_A + (\Delta \zeta)_L, \quad (14)$$

where

$$(\Delta \zeta)_A = -(\mathbf{n}_0 \times \boldsymbol{\beta}_p) \cdot \frac{(\mathbf{s}_p \times \mathbf{n}_0)}{|\mathbf{s}_p \times \mathbf{n}_0|}$$

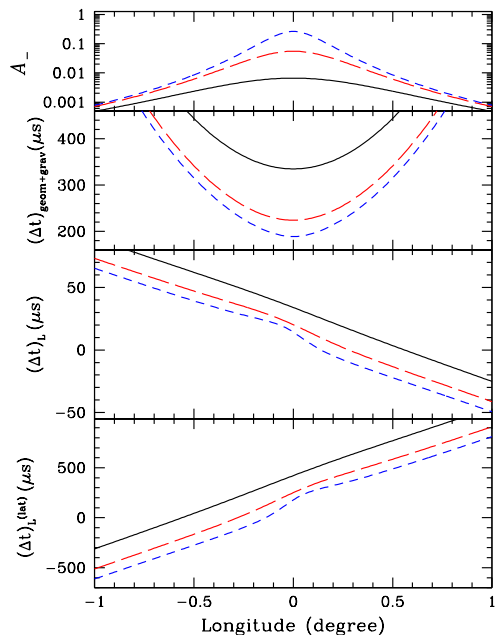


FIG. 2.— Same as Figure 1, except for the subdominant (“minus”) image.

$$= \frac{\Omega_b a_p}{c\sqrt{1-e^2}} [\cos i \sin \eta (\cos \psi + e \cos \omega) - \cos \eta (\sin \psi + e \sin \omega)], \quad (15)$$

$$(\Delta\zeta)_L = \frac{\Delta R_{\pm}(\mathbf{n}_0 \times \mathbf{r}) \cdot (\mathbf{s}_p \times \mathbf{n}_0)}{a_{\parallel} R} \cdot \frac{(\mathbf{s}_p \times \mathbf{n}_0)}{|\mathbf{s}_p \times \mathbf{n}_0|}$$

$$= - \left(\frac{\Delta R_{\pm}}{R} \right) \frac{r}{a_{\parallel}} (\cos \eta \cos \psi + \cos i \sin \eta \sin \psi) \quad (16)$$

are the contributions from aberration and lensing, respectively.

Unlike the longitudinal shift of the emission vector, the shift of colatitude affects the different components of pulse profile differently, thus changing the pulse profile periodically on the orbital timescale. In the following we consider for illustrative purposes a specific radio emission pattern based on the rotating vector model (RVM; Radhakrishnan & Cooke 1969) widely used for interpreting pulsar pulse profile and polarization data. In this model, the radio emission pattern consists of a set of cones which are circular in cross section as seen along the magnetic axis \mathbf{m} (see Fig. 3). As a result of pulsar rotation around \mathbf{s}_p , our line of sight \mathbf{n}_0 passes through the emission cone with half opening angle $\rho > |\zeta - \alpha|$ (where α is the angle between \mathbf{s}_p and \mathbf{m}) which causes two episodes of radio emission at the pulse phases $\pm\Phi_0$ corresponding to the leading and trailing edges of the cone⁷. Emission patterns close to circular edges are supported by theoretical ideas of pulsar emission mechanisms and observations of slow pulsars (Rankin 1993), although their occurrence in millisecond pulsars is not so clear (Kramer et al. 1998; Weisberg & Taylor 2002). The observed pulse profile of PSR J0737-3039A is consistent with a circular emission

⁷ The radio intensities of the two emission episodes are generally different because of the complicated azimuthal structure of the emitting region.

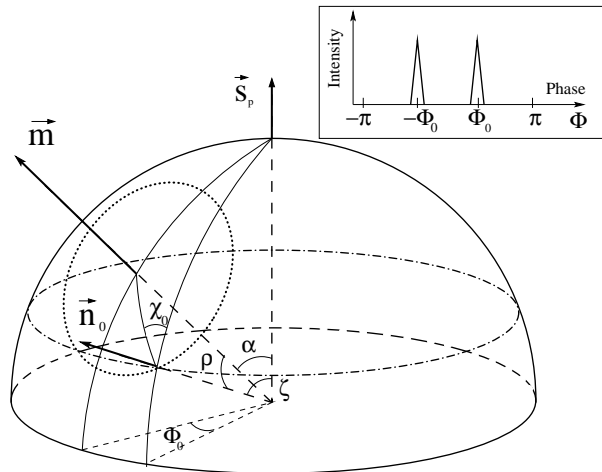


FIG. 3.— Geometry of pulsar emission with respect to the spin axis \mathbf{s}_p , magnetic axis \mathbf{m} , and our line of sight \mathbf{n}_0 . The latter cuts the celestial sphere and emission pattern (cone with opening angle ρ ; the dotted circle denotes its intersection with celestial sphere) along the dot-dashed line in the course of pulsar rotation, giving rise to features of the pulse profile at $\pm\Phi_0$, shown schematically in the inset.

pattern (Demorest et al. 2004; Manchester et al. 2005).

The full width of the pulse is $2\Phi_0$, with

$$\cos \Phi_0 = \frac{\cos \rho - \cos \zeta \cos \alpha}{\sin \zeta \sin \alpha}. \quad (17)$$

The variation of ζ then leads to a variation of Φ_0 :

$$\Delta\Phi_0 = \Delta\zeta \left(\frac{1}{\tan \Phi_0 \tan \zeta} - \frac{1}{\sin \Phi_0 \tan \alpha} \right). \quad (18)$$

It is easy to show that $\Delta\Phi_0$ is given by (which is also clear from Fig. 4)

$$\Delta\Phi_0 = - \frac{\Delta\zeta}{\sin \zeta \tan \chi_0}, \quad (19)$$

where χ_0 is the angle (on the celestial sphere) between the arc connecting \mathbf{n}_0 and \mathbf{s}_p and the arc connecting \mathbf{n}_0 and \mathbf{m} at the edges of the pulse, i.e., it coincides with the position angle of linear polarization and is given by the usual expression (Komesaroff 1970)

$$\tan \chi_0 = \frac{\sin \alpha \sin \Phi_0}{\cos \alpha \sin \zeta - \cos \Phi_0 \sin \alpha \cos \zeta}. \quad (20)$$

Equation (19) shows that in the framework of RVM the change of pulse width depends inversely on the change of position angle of radio polarization across the pulse. It also shows that while $\Delta\zeta$ is generally quite small ($\sim v_p/c \sim 10^{-3}$ due to aberration and $\sim \Delta R_{\pm}/a \sim 3 \times 10^{-3} \Delta R_{\pm}/R_E$ due to lensing), $\Delta\Phi_0$ can be significant when $\sin \zeta \tan \chi_0$ is small, as in the case of the PSR J0737-3039 system (see §3.3.2).

Note that the variation of the pulse profile on the orbital timescale due to the colatitudinal shift is not a unique property of RVM — this effect should exist for more complicated emission patterns as well. Interpretation of a positive detection of this effect in terms of pulsar spin geometry would be less straightforward for intricate beam shapes, and the exact relationship between $\Delta\Phi_0$ and χ_0 given by eq. (19) would also break down, but they do not affect our basic conclusion about the existence of such a phenomenon.

3.2. Latitudinal Time Delay

Standard pulsar timing formulae (including those discussed in §2) measure the arrival time of the *centroid* of radio pulses. However, pulse profile often has multiple components; in the rotating vector model these components correspond to passages of \mathbf{n}_0 through different emission cones (two for each cone). As discussed above, the variation of colatitude of emission direction due to aberration and lensing results in the change of the location (in phase) of a given pulse component relative to the pulse centroid. Thus if one times the arrival of a specific component of the pulse, additional delay associated with such shift of colatitude must be included; we call this “latitudinal delay”.

In RVM, the latitudinal delay associated with the leading edge of the pulse is⁸

$$(\Delta t)^{(\text{lat})} = \Delta\Phi_0/\Omega_p = (\Delta t)_A^{(\text{lat})} + (\Delta t)_L^{(\text{lat})}, \quad (21)$$

where $(\Delta t)_A^{(\text{lat})}$ and $(\Delta t)_L^{(\text{lat})}$ are contributions due to aberration and lensing. Using eqs. (15) and (19), we find the latitudinal aberration delay

$$(\Delta t)_A^{(\text{lat})} = C(\sin\psi + e\sin\omega) + D(\cos\psi + e\cos\omega) \quad (22)$$

where

$$\begin{Bmatrix} C \\ D \end{Bmatrix} = -\frac{\Omega_b a_p}{\Omega_p c \sqrt{1-e^2}} \frac{1}{\sin\zeta \tan\chi_0} \begin{Bmatrix} -\cos\eta \\ \cos i \sin\eta \end{Bmatrix}, \quad (23)$$

with $\tan\chi_0(\Phi_0)$ given by (20) in the framework of RVM. Similarly, using eq. (16), we find the latitudinal lensing delay

$$\begin{aligned} (\Delta t)_L^{(\text{lat})} &= \left(\frac{\Delta R_{\pm}}{R}\right) \frac{r}{a_{\parallel}} \frac{\cos\eta \cos\psi + \cos i \sin\eta \sin\psi}{\Omega_p \sin\zeta \tan\chi_0} \\ &\simeq -\left(\frac{\Delta R_{\pm}}{a_{\parallel}\Omega_p}\right) \frac{\Delta i \sin\eta + \Delta\psi \cos\eta}{\sin\zeta \tan\chi_0 [(\Delta i)^2 + (\Delta\psi)^2]^{1/2}}, \quad (24) \end{aligned}$$

where the second equality comes from expansion around $\psi = \pi/2 + \Delta\psi$ and $i = \pi/2 + \Delta i$.

Naturally, if one times the arrival of a specific component of pulse profile, then the total delay is the sum of the longitudinal contributions [eqs. (8), (10)] associated with the shift of the pulse centroid and the latitudinal contributions [eqs. (22), (24)] associated with pulse dilation/shrinkage. Thus, the combination of longitudinal and latitudinal delays results in (1) a uniform shift of the whole pulse profile in time by $(\Delta t)_A + (\Delta t)_L$ and (2) a nonuniform profile contraction/dilation, with each pulse component being shifted in phase by $\Delta\Phi_0 = \Omega_p[(\Delta t)_A^{(\text{lat})} + (\Delta t)_L^{(\text{lat})}]$. Pulse components closer to the pulse centroid (i.e. those with smaller Φ_0) are relatively more susceptible to contraction/dilation than the more distant components.

To evaluate $(\Delta t)^{(\text{lat})}$, a knowledge of ζ , χ_0 and η is necessary. Analysis of polarization data of PSR J0737-3039A constrains the angle between the spin axis and the magnetic axis to be $\alpha \approx 4^\circ$, while leaving ζ unconstrained (Demorest et al. 2004). The pulse profile of pulsar A exhibits remarkable similarity between its outermost leading and trailing edges (Demorest et al. 2004;

⁸ For the trailing edge, the delay is $-\Delta\Phi_0/\Omega_p$. Hereafter our formulae refer to the leading edge of the pulse.

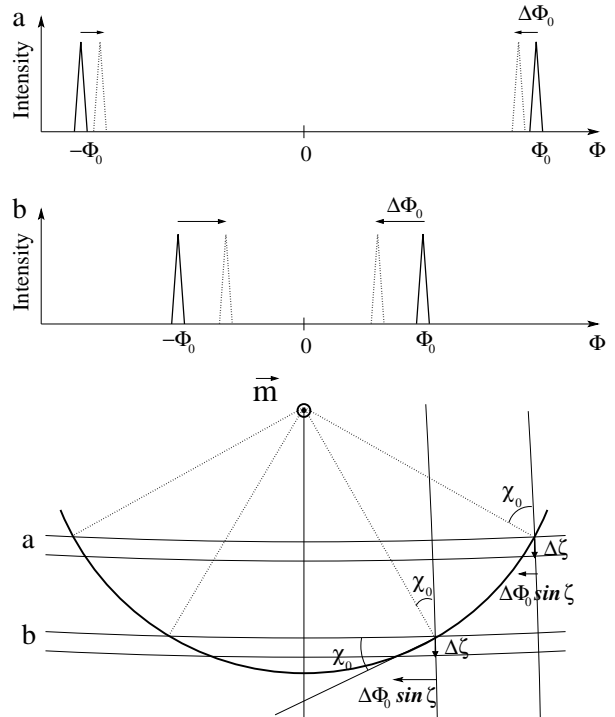


FIG. 4.— Variation of the pulse profile as a result of colatitudinal variation $\Delta\zeta$ for two different cuts of our line of sight \mathbf{n}_0 through the circular emission pattern. The bottom panel shows the projection onto the pulsar’s celestial sphere along the magnetic axis: the thick solid arc depicts part of the emission cone, the thin vertical arcs represent the magnetic projections of meridians, and the dotted lines denote the magnetic field lines, a and b denote the locus of two different lines of sight. This Figure illustrates how the proximity of our line of sight to the edge of the emission cone affects the total pulse width.

Manchester et al. 2005) at $\Phi_0 \approx 115^\circ$, which suggests that all profile components come from the same magnetic pole and that the two prominent spikes in the pulse profile can be associated with leading and trailing edges of the same emission cone. Based on the opening angle of other millisecond pulsars and $\zeta \sim \rho$, Demorest et al. (2004) suggests $\zeta \sim 50^\circ$, which we adopt in our estimate. Equation (20) then yields $\tan\chi_0 \approx 0.08$. Such small value of $\tan\chi_0$ results from the fact that in the Demorest et al. (2005) geometry our line of sight passes through the emission cone of pulsar A very close to its edge, see their Figure 3 for illustration.

The bottom panels of Figures 1 and 2 depict the lensing latitudinal delay $(\Delta t)_L^{(\text{lat})}$ for both images. Clearly, because of the small value of $\tan\chi_0$ for the PSR J0737 system, $(\Delta t)_L^{(\text{lat})}$ is much larger than $(\Delta t)_L$ and reaches $\approx 79 \mu\text{s}$ for $i = 90.28^\circ$. In binary systems with smaller inclination angles satisfying $a_{\parallel}|\Delta i| \gg R_E$ the maximum amplitude of $(\Delta t)_L$ reached at $\Delta\psi \approx \Delta i(1 - \sin\eta)/\cos\eta$ is given by

$$\max|(\Delta t)_L^{(\text{lat})}| \approx \frac{(R_E/a_{\parallel})^2}{2|\Delta i|\Omega_p \sin\zeta \tan\chi_0} (1 + \sin\eta), \quad (25)$$

for $e \ll 1$. Scaling of $\max|(\Delta t)_L^{(\text{lat})}|$ with $|\Delta i|$ is analogous to that of $\max|(\Delta t)_L|$. For $i = 88.7^\circ$ and spin-magnetic orientation of pulsar A adopted here one finds

$\max|(\Delta t)_L^{(\text{lat})}| \approx 22 \mu\text{s}$ (which is likely still measurable) reached ≈ 13 s before conjunction, which is at the ingress of eclipse of pulsar A.

Another constraint on the pulsar A spin orientation (independent from the polarization measurements) comes from the observed lack of profile variation of A which should occur in general because of A's geodetic precession (Manchester et al. 2005). Stability of A's pulse profile suggests that A may currently be at a special precessional phase with its spin axis almost coplanar with both the orbital angular momentum axis and our line of sight \mathbf{n}_0 , implying $\eta \sim 90^\circ$. Assuming this Manchester et al. (2005) have determined the region of α - ζ phase space compatible with A's pulse profile stability. A wide range of α is allowed, including the small- α solution preferred by Demorest et al. (2004). In Table 1 we list the values of timing coefficients A , B , C , D , together with the maximum amplitudes of longitudinal and latitudinal lensing delays (for $i = 90.28^\circ$) for several spin orientations of A suggested by Demorest et al. (2004) and Manchester et al. (2005), assuming for illustrative purposes that in the latter case $\eta = 85^\circ$. Clearly, for small α (hence small $\tan \chi_0$), the latitudinal delays are much larger than the longitudinal ones, although the latitudinal aberration delay is reduced for $\eta \sim 90^\circ$ (while the magnitude of the latitudinal lensing delay is largely unaffected). For illustrative purposes, in the rest of the paper we will focus on the small- α solution (Demorest et al. 2004).

3.3. Effect of Double Images

In addition to the pulse profile change due to the change of emission colatitude (see §3.3.1), gravitational lensing affects pulse profile in another way. Near the orbital conjunction, light bending splits the source (pulsar) into two radio images in the plane of the sky. The displacement of the image from the source is ΔR_\pm , as given by eq. (3), and the image magnification \mathcal{A}_\pm given by eq. (12). While aberration affects the arrival time of both images in the same way, lensing breaks this degeneracy and separates the arrival times of two weighted replicas of the unperturbed pulse profile. Assuming that in the absence of orbital motion and lensing the pulse profile is given by $I_0(\Phi)$, we find that the observed pulse profile at orbital phase ψ , including the light bending effect, is

$$I(\Phi; \psi) = \mathcal{A}_+ e^{-\tau_+} I_0(\Phi - \Omega_p \Delta t_+) + \mathcal{A}_- e^{-\tau_-} I_0(\Phi - \Omega_p \Delta t_-), \quad (26)$$

where the factors $e^{-\tau_\pm}$ accounts for the absorption of pulsar signal by plasma in the magnetosphere of companion. The time delays Δt_\pm for both images include not only the rotational contributions [eqs. (8), (10), (22) and (24)], but also the geometric delay and the (modified) Shapiro delay (see Lai & Rafikov 2005). Note that \mathcal{A}_\pm , τ_\pm , Δt_\pm are all functions of the orbital phase ψ .

For illustrative purposes, we assume $\tau_+ = \tau_-$, and show in Figure 5 the relative contributions of the two images in shaping the pulse profile $I(\Phi)$ near the orbital conjunction for $i = 90.28^\circ$. In practice, one could adopt a simple procedure when analyzing arrival times near conjunction: since the “+” image dominates the lightcurve, one would naturally assume that the timing residual due to lensing is primarily given by Δt_+ and the negative

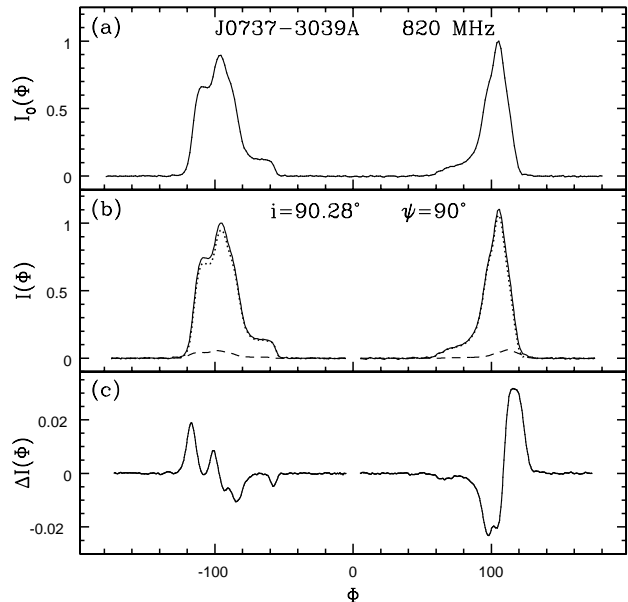


FIG. 5.— (a) Pulse profile of J0737-3039A far from conjunction, $I_0(\Phi)$. (b) Contributions to the total pulse profile $I(\Phi)$ (solid curve) at conjunction ($\psi = 90^\circ$) due to the positive (dotted curve) and negative lensed image (dashed curve) taking into account different time delays and magnifications of the images. In the calculation $i = 90.28^\circ$, $\zeta = 50^\circ$, $\eta = 45^\circ$, and $\alpha = 4^\circ$ are assumed. (c) Difference between $I(\Phi)$ and $I_0(\Phi)$, with the latter magnified by $\mathcal{A}_+ + \mathcal{A}_-$ and shifted by Δt_+ in time at conjunction. The remaining residuals are due to the improperly subtracted negative image and are rather small. The flux units in the three panels are the same.

image contributes to the pulse profile mainly through its magnification. Figure 5c depicts the relative error incurred by this assumption: we plot the difference between I_0 magnified by $\mathcal{A}_+ + \mathcal{A}_-$ and shifted by Δt_+ in time and the real profile $I(\Phi)$ which properly includes contributions from both images at conjunction. One can see that this simple procedure does perform quite well, and the flux residuals due to improper subtraction of the negative image are at most several percent. In reality, since the light of “-” image passes closer to the companion star than the light of “+” image, and the magnetospheric absorption depends strongly on the plasma density, we expect that near conjunction, τ_- is much greater than τ_+ . This would further decrease the contribution of the “-” image to the distortion of the pulse profile.

4. DETECTABILITY OF ROTATIONAL DELAYS AND PULSE DISTORTION

The rotational time delays discussed in previous sections could be observed in different ways. The aberration effect results in arrival time variation and pulse distortion throughout the whole cycle of the orbital motion, while the lensing effect is important only in very edge-on systems near the superior conjunction of the pulsar. As discussed above, the pulse profile and polarization of PSR J0737-3039A imply that our line of sight crosses the edge of the pulsar's emission cone (Demorest et al. 2004), resulting in significant pulse distortion and the associated latitudinal delay. For exam-

ple, taking $\zeta = 50^\circ$, $\tan \chi_0 = 0.08$ and $i = 90.28^\circ$, we find, for the aberration delays, $A = -4.7 \sin \eta \mu\text{s}$, $B = 0.023 \cos \eta \mu\text{s}$, $C = 59 \cos \eta \mu\text{s}$ and $D = 0.3 \sin \eta \mu\text{s}$. The lensing delays are shown in Figures 1 and 2. Aberration results in fractional pulse width variation of order $\Delta\Phi_0/\Phi_0 = \Omega_p(\Delta t)_A^{(\text{lat})}/\Phi_0 \sim \Omega_p C/\Phi_0 \sim 10^{-2} \cos \eta$ in the course of the pulsar’s orbital motion. For a few seconds around the superior conjunction, light bending gives rise to additional profile distortion at a similar level.

Motivated by our results, we propose to perform timing of *separate components* of the pulse profile to detect pulse dilation/contraction and the associated latitudinal delays. Instead of fitting one template to the whole observed pulse profile to determine its overall timing displacement (or the arrival time of the pulse centroid), one can directly fit templates for each individual component of the profile. Assuming that some pairs of components represent the leading and trailing edges of the emission cone through our line of sight, one can measure the difference between their times of arrival and correlate its variation with the orbital phase. This method presents a relatively easy way of measuring the latitudinal delays and extracting pulsar parameters from them. In the case of PSR J0737-3039A, periodic profile distortions must be very strong because of the small ($\sim 4^\circ$) magnetic inclination angle of pulsar A with respect to its spin (Demorest et al. 2004). The latitudinal delay is of order $C = 59 \cos \eta \mu\text{s}$, which should be detectable since RMS timing residuals of pulsar A are already at the level of $27 \mu\text{s}$ (Lyne et al. 2004). Such detection would directly constrain χ_0 , ζ and η .

Detection of the standard “longitudinal” aberration delay (eqs. [8]-[9]) is a more difficult task. Damour & Deruelle (1986) were the first to recognize that this delay cannot be observed directly as a timing variation on the orbital time scale since it can be fully absorbed into the Roemer delay by rescaling/redefining the eccentricity, semimajor axis, epoch of periastron and two other post-Newtonian parameters. More precisely, because of the aberration delay, the observed values of the semimajor axis a^{obs} , eccentricity e^{obs} , and the epoch of periastron T_0^{obs} are related to the true values of these quantities a^{true} , e^{true} , T_0^{true} by the formulae

$$\frac{a^{obs}}{a^{true}} = \frac{e^{obs}}{e^{true}} = 1 + \epsilon_A,$$

$$\epsilon_A \equiv \frac{cA}{a_p \sin i} \approx -3.3 \times 10^{-6} \sin \eta, \quad (27)$$

$$T_0^{obs} = T_0^{true} - \sqrt{1 - e^2} \Omega_b^{-1} \epsilon_B,$$

$$\epsilon_B \equiv \frac{cB}{a_p \sin i} \approx 1.6 \times 10^{-8} \cos \eta. \quad (28)$$

where the numbers are for the J0737-3039 system. The degeneracy with Roemer delay implies that to detect aberration delay one must look for arrival time variation over longer timescales. As a result of geodetic precession, both angles η and ζ , and thus a^{obs} , e^{obs} , T_0^{obs} will change with amplitude $\sim \epsilon_A, \epsilon_B$, on the timescale of the precession period. In some systems the precession can be rather rapid (with period of tens of years) and, if ϵ_A, ϵ_B are not too small, this variation can be detected in long-term observations and the pulsar spin orientation can be inferred (Stairs et al. 2004). Such measurement would

be complicated by the fact that variable aberration is not the only contribution to the evolution of a and e : they would also evolve because of the gravitational wave emission and possible time-dependent Doppler shift of the system, see DT92. However, these additional contributions should give rise to linear non-periodic trends in \dot{a} and \dot{e} making it possible to disentangle their effect in long-term timing observations from periodic (nonlinear) behavior of aberration time delay.

In the case of the PSR J0737-3039 system, the precession period of pulsar A is 75 yr, and the relative variation of observed eccentricity and semimajor axis on this timescale is $3.3 \times 10^{-6} \sin \eta$, while the observed epoch of periastron varies by $22 \mu\text{s}$. The current timing accuracy of J0737-3039A (Stairs 2005, private communication) allows determination of e^{obs} and a^{obs} with relative accuracy of 1.7×10^{-5} and 1.4×10^{-6} , respectively, and the measurement of T_0^{obs} has absolute accuracy of 35 ms. Thus, it would in principle be possible to detect variation of a^{obs} (but not of e^{obs} or T_0^{obs}) caused by geodetic precession and longitudinal aberration at a 2σ level after tens of years of timing observation.

Much better measurement can be made if one monitors the long-term drift of timing positions of *individual* pulse features instead of the whole profile. Then the amplitude of drift⁹ in a^{obs} , e^{obs} , T_0^{obs} caused by geodetic precession is augmented by the much more significant latitudinal aberration. Since the latitudinal delay has the same dependence on the orbital elements as the longitudinal one, its effect on variation of a^{obs} , e^{obs} , T_0^{obs} can be included by simply changing $A \rightarrow A + C$ and $B \rightarrow B + D$ in (27) and (28). As a result, a^{obs} and e^{obs} determined from timing of individual pulse features vary on geodetic precession timescale with relative amplitude $4.2 \times 10^{-5} (\cos \eta - 0.08 \sin \eta)$. This should give a highly significant detection of geodetic variation of a^{obs} (and on a shorter baseline than the longitudinal aberration variation) and yield a measurement of e^{obs} variation at a 2σ level. The accompanying variation of T_0^{obs} at the level of 0.4 ms would still escape detection.

Time delays caused by gravitational light bending do not suffer from the degeneracy with Roemer delay (or any other timing contribution¹⁰) because of their unique time dependence (see eqs. [10], [24], and Figs. 1-2). As noted before, in general the rotational lensing delay is asymmetric with respect to the conjunction, which may facilitate the separation of this delay from the geometric delay and the (corrected) Shapiro delay (Lai & Rafikov 2005). For the parameters adopted in Figure 1, the maximum amplitude of $(\Delta t)_L$ for the positive image is $\sim 5 \mu\text{s}$ (for $i = 90.28^\circ$ or the minimum $R = 4000 \text{ km}$), while $(\Delta t)_L^{(\text{lat})}$ reaches as high as $70 \mu\text{s}$, both achieved within several seconds of conjunction. The latter delay would be detectable if one times the arrival of individual features of the pulse profile.

Detecting the lensing-related time delays may be a challenging task. One factor which limits the accuracy

⁹ In this approach the orbital parameters should be determined separately for each pulse component.

¹⁰ The only degeneracy is with the frame-dragging delay caused by the companion’s spin (Wex & Kopeikin 1999; Raffikov & Lai 2005) but in binaries consisting of two neutron stars the frame-dragging delay is always negligible.

of pulsar timing arises from the intrinsic variation of the pulse profile from one pulse to the next. If one times the arrival of a pulse feature with width w , then the timing accuracy after combining N_p pulses is $\sigma_t \sim w/\sqrt{N_p}$. For PSR J0737-3039A, the pulse has two peaks, each with width $w \sim 4$ ms. The lensing effect lasts about ~ 4 s, so that in each orbit there are $N_p \sim 200$ pulses during the lensing event, and about half of them¹¹ may be used for timing purposes. This gives $\sigma_t \sim 0.4$ ms for a single passage through conjunction, somewhat larger than the amplitude of $(\Delta t)_L^{(\text{lat})}$ (for $i = 90.29^\circ$). By adding up pulses from many orbits one will obtain better timing accuracy which may make the detection of $(\Delta t)_L^{(\text{lat})}$ possible. This would set a robust constraint on the system's inclination angle.

Finally, all rotational effects (both aberration and lensing) that we described in application to J0737-3039A should also be relevant for J0737-3039B. Since the masses of the two pulsars are quite similar, the variation of the direction of emission vector $\Delta \mathbf{N}$ is also similar for both pulsars, but the spin period of pulsar B, $P_B = 2.8$ s is significantly longer than $P_A = 23$ ms. As a result, the amplitudes of all spin-dependent delays for pulsar B are $\sim 10^2$ higher than for pulsar A. However, the current timing accuracy of pulsar B, 2.7 ms (Lyne et al. 2004), is much poorer than that of pulsar A and is not expected to improve significantly in the future. The pulse profile of pulsar B is unstable and subject to variations throughout the orbit, presumably due to the influence of the intense wind/radiation from pulsar A (Ramachandran et al. 2004). Moreover, the spin and magnetic geometry of pulsar B (not well constrained observationally at present) may not be very favorable for exhibition of large latitudinal effects¹².

5. DISCUSSION

Pulse profile distortion associated with the latitudinal aberration delay is the most easily measurable among all rotational timing effects in J0737-3039A if the spin-magnetic orientation of this pulsar inferred by Demorest et al. (2004) is correct. This effect should be detectable with the current timing accuracy if the arrival times of individual pulse components (rather than the pulse centroid) are monitored. However, if this effect is not found in the data, we can suggest two possible reasons. First, it is conceivable that at the present time the spin orientation is such that $\cos \eta \ll 1$, resulting in a rather small profile distortion by aberration (see eq. [23]). This would additionally account for the remarkable stability

¹¹ Lensing effects manifest themselves only very near the conjunction (when $R \sim R_E$) where absorption by magnetospheric plasma of pulsar B is important (Kaspi et al. 2004; Rafikov & Goldreich 2004). At the same time, McLaughlin et al. (2004) and Lyutikov & Thompson (2005) have demonstrated that even very close to A's superior conjunction radio signal of A can still pass through B's magnetosphere almost unattenuated at some intervals of B's rotation phase within which at least several rotational periods of A can be detected. It is this penetrating part of A's radio flux that can be used to search for gravitational lensing effects in J0737-3039.

¹² A detailed modeling of the modulation of the pulsar A eclipse by pulsar B's rotation yields the following parameters for pulsar B: the angle between the spin axis and magnetic axis $\sim 75^\circ$, the inclination of the spin axis to the orbital angular momentum axis $\sim 60^\circ$ (Lyutikov & Thompson 2005).

of J0737-3039A pulse profile (Manchester et al. 2005). However, such a situation would not last since geodetic precession of the pulsar spin axis changes η on the timescale of years, so that several years from now latitudinal aberration should become observable. There is also a possibility that the spin of pulsar A is almost aligned with the orbital angular momentum¹³ which, because of the edge-on orientation of the system, would naturally make $\cos \eta \ll 1$. This requires a very large opening angle of the emission cone, $\rho \sim 90^\circ$, which may be unlikely. Second, it is possible that the spin and magnetic orientations inferred by Demorest et al. (2004) are incorrect, e.g. because of the failure of RVM. This would not be very surprising given that the polarization data are corrupted by quasi-orthogonal modes. Even the interpretation of the emission as coming from a single magnetic pole can be called into question¹⁴. If this were the case, the angles α and ζ could be different from what we used in our estimates, possibly reducing the magnitude of pulse distortion. Thus, measuring the pulse variation in J0737-3039A on the orbital timescale can be used to probe the emission and spin geometry of pulsar A.

Pulse shape variations caused by latitudinal shifts are very promising from the observational point of view: unlike the lensing effects, profile dilation due to orbital aberration does not require special orientation of orbital plane which makes it potentially observable in many binary systems. As far as we are aware, no one has attempted to detect pulse profile expansion/contraction of the predicted form correlated with the phase of pulsar orbital motion. The only possible exception is the study of PSR B1534+12 by Stairs et al. (2004) in which pulse shape variations were detected through fitting a linear combination of two standard profiles to all observed profiles. Variation of coefficients of this linear combination on short (orbital) and long (geodetic precession) timescales allowed Stairs et al. to set constraints on the pulsar spin geometry. This procedure seems to be less straightforward than a direct measurement of the variation of the phase separation between different pulse components that we propose to perform, although it has an advantage of yielding pulsar spin orientation free from assumptions about the beam geometry.

It may be possible to infer the PSR J0737-3039A spin orientation from rotational effects alone, without resorting to polarimetric observations. The pulse profile variations on the orbital timescale and the long-term geodetic variations of orbital parameters may be enough to measure A's spin orientation with respect to its magnetic axis (angle α) and with respect to orbital angular momentum of the binary. Detection of lensing effects would refine the accuracy of such measurement and additionally constrain the inclination of the system, and may also help verify the assumption of circular beam shape.

Rotational delays may be measurable in other compact binary pulsar systems with significant v/c . In such systems pulse profile variations on orbital timescales may be a telltale signature of latitudinal aberration. The effect

¹³ The natal kick on pulsar B (e.g. Willems et al. 2004) would in general make \mathbf{s}_A misalign with the orbital angular momentum axis except if the kick was directed along or close to the orbital plane.

¹⁴ This would also affect constraints obtained by Manchester et al. (2005) which were derived assuming single pole configuration.

TABLE 1. TIME DELAYS FOR VARIOUS SPIN GEOMETRIES OF J0737-3039A.

α	ζ	η	$\tan \chi_0$	$A, \mu\text{s}$	$B, \mu\text{s}$	$C, \mu\text{s}$	$D, \mu\text{s}$	$\max (\Delta t)_L , \mu\text{s}$	$\max (\Delta t)_L^{(\text{lat})} , \mu\text{s}$
4°	50°	45°	0.081	-3.4	0.016	42.0	0.20	5.8	72
18.7°	78.5°	85°	0.31	-3.7	0.0016	1.1	0.059	3.1	17
5.7°	83.7°	85°	0.091	-3.7	0.0016	3.5	0.20	3.0	56
34.2°	42.3°	85°	0.88	-5.4	0.0023	0.54	0.030	4.5	8.4

is strongest for pulsars in which the polarization angle of radio signal does not exhibit significant variation across the pulse profile, implying small value of $\tan \chi_0$ and large $\Delta\Phi_0$ (see eq. [19]). This could serve as a useful criterion for selecting potential targets to detect orbital pulse profile variations (geodetic variations will also be enhanced for such pulsars by latitudinal effects, see §4). Timing of individual pulse components needed for such detection should be facilitated in pulsars with rich pulse profiles exhibiting many symmetric sharp features. Using this technique to measure pulsar orientation with high significance may require stacking together observations obtained in many orbits¹⁵, but, presumably, this would still require much shorter baseline than is needed for detection of timing variations caused by geodetic precession.

Our results on the lensing effects have been obtained in the static approximation, which neglects the change in the orbital configuration of the binary during the time it takes a radio photon emitted by pulsar A to cross the system. This is the approach adopted by Damour &

Taylor (1992) and many other authors since then. Recently Kopeikin & Schäfer (1999) have gone beyond the conventional static approximation and presented ways of including the effect of finite photon propagation time on pulsar timing. We plan to investigate the influence of this effect on lensing timing signals in the future (Rafikov & Lai 2005).

We thank Jim Cordes and Ingrid Stairs for useful discussion and Vicky Kaspi and Rene Breton for making data on pulse profile of J0737-3039A available to us. We are grateful to an anonymous referee for useful suggestions which improved this manuscript. RRR thankfully acknowledges the financial support by the W. M. Keck Foundation and NSF via grant PHY-0070928. DL thanks CITA and TIARA (Taiwan) for hospitality and is supported in part by NSF grant AST 0307252 and NASA grant NAG 5-12034.

¹⁵ Time interval during which such observations are taken must be small compared to the geodetic precession period since otherwise

system's geometry would change.

REFERENCES

- Arons, J., Backer, D. C., Spitkovsky, A., & Kaspi, V. 2004, in *Binary Radio Pulsars*, ASP Conf. Series; eds. F. A. Rasio & I. H. Stairs (astro-ph/0404159)
- Blandford, R. & Teukolsky, S. A. 1976, *ApJ*, 205, 580
- Burgay, M., D'Amico, N., Possenti, A. et al. 2003, *Nature*, 426, 531
- Coles, W. A., McLaughlin, M. A., Rickett, B. J. et al. 2005, *ApJ*, 623, 392
- Damour, T. & Deruelle, N. 1986, *Ann. Inst. Henri Poincaré*, 44, 263
- Damour, T. & Taylor, J. H. 1992, *Phys. Rev. D*, 45, 1840 (DT92)
- Demorest, P. et al. 2004, *ApJ*, 615, L137
- Doroshenko, O. V. & Kopeikin, S. M. 1995, *MNRAS*, 274, 1029
- Goicoechea, L. J. et al. 1995, *A&A*, 303, 502
- Kaspi, V., Ransom, S., Backer, D. C. et al. 2004, *ApJ*, 613, L137
- Klioner, S. A. & Kopeikin, S. M. 1992, *AJ*, 104, 897
- Komesaroff, M. M. 1970, *Nature*, 225, 612
- Kopeikin, S. M. & Schäfer, G. 1999, *Phys. Rev. D*, 60, 124002
- Kramer, M., Xilouris, K. M., Lorimer, D. R., Doroshenko, O., Jessner, A., Wielebinski, R., Wolszczan, A., & Camilo, F. 1998, *ApJ*, 501, 270
- Lai, D. & Rafikov, R. R. 2004, *ApJ*, 621, 41L
- Lyne, A. G. et al. 2004, *Science*, 303, 1153
- Lyutikov, M. & Thompson, C. 2005, *ApJ*, 634, 1223
- Manchester, R. N. et al. 2005, *ApJL*, 621, L49
- McLaughlin, M. A. et al. 2004, *ApJ*, 613, L57
- Radhakrishnan, V. & Cooke, D. 1969, *ApL*, 3, 225
- Rafikov, R.R., & Goldreich, P. 2005, *ApJ*, 631, 488
- Rafikov, R.R., & Lai, D. 2005, *ApJ*, accepted, astro-ph/0512417
- Ramachandran, R., Backer, D. C., Demorest, P., Ransom, S., & Kaspi, V. 2004, astro-ph/0404392
- Rankin, J. M. 1993, *ApJ*, 405, 285
- Ransom, S. et al. 2004, *ApJ*, 609, L71
- Schneider, J. 1990, *A&A*, 232, 62
- Smarr, L. L. & Blandford, R. 1976, *ApJ*, 207, 574
- Stairs, I., Thorsett, S. E., & Arzoumanian, Z. 2004, *Phys. Rev. Lett.*, 93, 141101
- Weisberg, J. M. & Taylor, J. H. 2002, *ApJ*, 576, 942
- Wex, N. & Kopeikin, S. M. 1999, *ApJ*, 514, 388
- Willems, B., Kalogera, V., & Henninger, M. 2004, *ApJ*, 616, 414